Pure Appl. Chem., Vol. 81, No. 9, pp. 1645–1653, 2009.
doi:10.1351/PAC-CON-08-10-10
© 2009 IUPAC, Publication date (Web): 10 August 2009

Near-field optical probes provide subdiffraction-limited excitation areas for fluorescence correlation spectroscopy on membranes*

Dusan Vobornik[1], Daniel S. Banks[2], Zhengfang Lu[1], Cécile Fradin[2], Rod Taylor[1], and Linda J. Johnston[1,‡]

[1]Steacie Institute for Molecular Sciences, National Research Council of Canada, Ottawa, Ontario K1A 0R6, Canada; [2]Department of Physics and Astronomy, McMaster University, Hamilton, Ontario L8S 4M1, Canada

Abstract: Near-field optical probes have been used to produce a subdiffraction-limited observation area for fluorescence correlation spectroscopy (FCS) experiments on supported membranes. The design of a bent, etched fiber probe that is compatible with biological imaging in an aqueous environment is described. This probe design is used for proof of principle experiments to measure lipid diffusion in a fluid-supported bilayer. A reduction in excitation area of approximately one order of magnitude (relative to a confocal FCS experiment) is obtained with a probe aperture diameter of 140 nm. We also demonstrate a simple approach for modeling the autocorrelation decay due to diffusion within the excitation profile at the near-field scanning optical microscopy (NSOM) probe aperture. The use of probes with smaller apertures is expected to provide an additional order of magnitude reduction in the observation area, thus enabling the study of cellular membranes with higher concentrations of fluorophores than is currently possible with diffraction-limited techniques.

Keywords: bilayers; fluorescence correlation spectroscopy; near-field scanning optical microscopy; single-molecule dynamics.

INTRODUCTION

Fluorescence correlation spectroscopy (FCS) is a powerful method for measuring single-molecule dynamics and has been widely used to obtain concentrations, diffusion coefficients, rate constants, and association/dissociation constants [1,2]. FCS measurements typically use diffraction-limited optics of a confocal microscope to probe single-molecule dynamics in fluids using femtoliter (10^{-15} l) observation volumes or in membranes using observation areas less than 1 μm^2. Since FCS relies on the temporal analysis of fluctuations of the fluorescence signal, it is essential to have at most only a few molecules in the detection volume. Current confocal detection volumes limit the concentrations to the picomolar to nanomolar range. Since typical concentrations of biomolecules are often in the micro to millimolar range, various methods have been applied in attempts to reduce the observation volume for FCS measurements. These include the use of a total internal reflection geometry [3] and application of a supercritical angle objective to reduce the axial dimension of the observation volume [4]; however, the re-

*Paper based on a presentation at the XXII[nd] IUPAC Symposium on Photochemistry, 28 July–1 August 2008, Gothenburg, Sweden. Other presentations are published in this issue, pp. 1615–1705.
‡Corresponding author

duction in the axial direction for the supercritical objective results in an increase in the radial direction. Stimulated emission depletion (STED), a method based on the use of a second shaped laser pulse to stimulate emission of the outer edges of a diffraction-limited excitation spot created by an initial laser pulse, has achieved a five-fold decrease in the observation volume [5]. More substantial reductions have been obtained using subwavelength-sized apertures (holes) in thin films to produce attoliter (10^{-18} l) [6,7], as well as zeptoliter (10^{-21} l) observation volumes (the latter corresponding to an observation area in lipid membranes of 0.002–0.03 μm^2) [7–9]. Such approaches have significant promise for measurements in solution, as, for example, for single-molecule enzymology [9,10], and have also recently been applied to cellular imaging [7,11]. Nevertheless, their applicability to studies in cells is likely to be significantly limited by the requirement for growing cells on the metal films used to construct the apertures and for membrane invagination into the subwavelength diameter apertures, which dramatically restricts the membrane area that can be probed.

The use of near-field optical probes to reduce the excitation volume/area for FCS measurements has been suggested in several recent reviews [12,13], and should in principle be compatible with reductions comparable to those achieved using arrays of apertures in metal films. Near-field scanning optical microscopy (NSOM) provides subdiffraction-limited optical resolution for biological imaging and is typically implemented using an optical fiber probe as an excitation source [13,14]. The optical resolution is controlled by the diameter of the probe aperture with typical values ranging from 50 to 100 nm. The application of near-field optical probes for FCS measurements on cellular membranes is expected to provide a substantial advantage over the use of arrayed subwavelength apertures since one has the ability to image the cell surface at high spatial resolution [15–17], in order to identify areas of interest, prior to conducting FCS measurements on targeted areas of the membrane. Although FCS has been successfully reported using an untapered fiber optic probe [18], the use of fiber-based optical probes with nanometer-sized apertures has only recently been demonstrated in our laboratories [19]. This article reviews our recent advances toward fabrication of near-field optical probes for biological imaging [20] and our initial demonstration of the utility of these probes for FCS measurements in 2D membranes with subdiffraction-limited resolution [19].

BENT FIBER PROBES FOR FCS-NSOM

High GeO_2-doped single-mode fibers, obtained from Mitsubishi Inc., were used to make the NSOM probes. The fibers had a core diameter of 3 μm and core plus clad diameter of 125 μm. An 80° multistep bend (illustrated in Fig. 1A) was made approximately 1 mm from one end of a 0.8-m-long piece of the fiber [20]. This was accomplished using a spark-discharge-based bending apparatus which formed a radiused bend without twisting or damaging the fiber. We separately placed the end of the probe into the spark-discharge to form a hemi-spherically radiused profile as shown in Fig. 1B. The bent fiber probe was then submerged in buffered oxide etchant. Since these fibers had an approximately parabolic dopant profile over the core, preferential etching of the cladding relative to the core resulted in the production of a ~3 μm basewidth, ~3 μm high conical tipped structure (shown in Figs. 1B and 1C) [20]. The etching procedure also provided a wide (60°) cone angle near the end of the tip for improved light throughput.

The 66-μm-diameter etched probes were then totally metalized with a ~300-nm-thick coating of Al. An optical aperture was created at the tip of the conical structure using a focused ion-beam (FIB) to nanoslice off the desired amount of Al (a typical aperture is shown in Fig. 1C). We routinely record a scanning electron microscopy (SEM) image of the aperture area for each of our NSOM probes during the FIB milling production step. To further confirm the size and shape of the aperture down on the sample surface, we image a test sample consisting of dye-labeled 40-nm-diameter spheres spin-coated in a thin (around 30 nm) polymer film deposited on a glass cover slip. The full width half maximum size of the smallest features in such a scan approximates the probe aperture diameter. In the case of the probe used for the FCS-NSOM data shown in this paper, a cross-section for the smallest feature in a

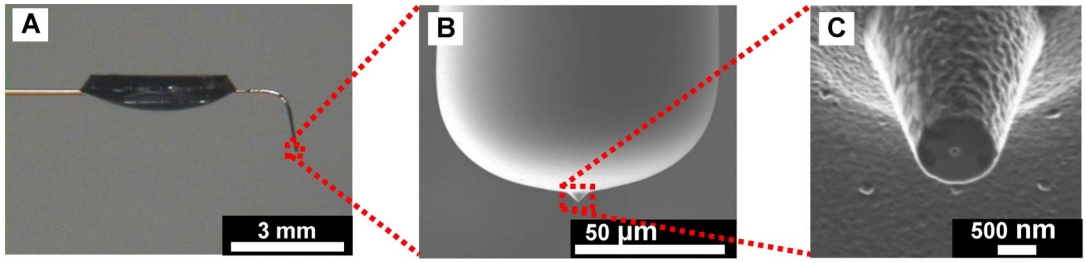

Fig. 1 Bent fiber NSOM probe: (a) fiber probe glue-mounted on an AFM stub, (b) SEM image of tip region, and (c) SEM image of FIB milled conical structure showing the optical aperture.

$10 \times 10\ \mu m^2$ image of dye-labeled spheres gives a value of 138 nm in good agreement with SEM data for the aperture (diameter estimated at 140 nm). A previous calibration curve for similar etched probes without the hemispherical profile showed that the transmission efficiency varied from 0.1 to 5 % for apertures ranging in diameter from 100 to 200 nm [20]. The hemispherical profile is an advantage for scanning samples with relatively large changes in topography, such as cell surfaces.

The nanoslicing results in a 600-nm-diameter nanometrically flat-topped probe tip. Provided the conical structure can be brought down close to normal (i.e., within a few degrees) to the sample surface, the aperture will effectively be in contact with the surface, ensuring that the sample is entirely within the near-field of the evanescent light field emerging from the probe aperture. The relatively large diameter of the flat-topped tip results in poor atomic force microscopy (AFM) topography, which fortunately is not an issue for flat membrane samples. In principle, the use of an FIB to drill a hole through the Al coating at the apex of the conical structure would avoid this problem. However, as was observed a number of years ago [21] and more recently [22], the rather large grain size of the Al coating can give false indications to where the apex is when imaging directly down onto the conical structure. The large flat region of the tip does serve to decrease the tip pressure on the sample surface, a feature which will be very important for minimizing damage during FCS-NSOM experiments on cells.

The bent, etched, metalized, and FIB'd fiber was then glue-mounted onto an AFM stub to form a cantilever (Fig. 1A) which can be used on any standard laser deflection distance-regulated AFM. The spring constant of the fiber probe is estimated to be ~200 N/m, making it a rather stiff cantilever. The cantilever is vibrated vertically at ~20 kHz using a z-piezoelectric driver (i.e., tapping or intermittent contact mode) to avoid producing damaging shear forces on the surface of the sample. Experiments were carried out on a combined AFM/NSOM microscope based on a Digital Instruments Bioscope mounted on an inverted fluorescence microscope (Zeiss Axiovert 100). A continuous-wave mixed-gas ion laser (Coherent, Innova 70 Spectrum) was used for excitation purposes (488 nm, 7–20 mW). For FCS experiments, typically 0.1–4 mW is incident on the cleaved end of the optical fiber probe, and the coupling efficiency is approximately 50 %. Fluorescence was collected with a 63× objective (0.75 NA), with appropriate filters to remove residual excitation (488-nm notch filter from Kaiser Optical Systems and band-pass filter 535AF26 from Omega Optical), and detected using an avalanche photodiode detector (Perkin-Elmer Optoelectronics, SPCM-AQR-15). Fluorescence was collected for 45–120 s for each measurement. To calculate the correlation data, the fluorescence signal from the avalanche photodiode detector was sent to a multi-tau correlator (Flex03LQ-12, correlator.com).

Recent work in our laboratories has demonstrated the utility of this NSOM probe design for fluorescence imaging of dry lipid monolayers and supported lipid bilayers in an aqueous environment with spatial resolutions below 100 nm [23–25]. We have also used this probe design for imaging cell surfaces, resolving nanoscale distributions of several membrane proteins and lipid domains [15–17]. An example illustrating our ability to resolve nanometer-sized caveolae membrane domains in fixed cells is shown in Fig. 2. The fluorescence image shows many small, roughly circular fluorescent features that vary between 60 and ~200 nm in diameter. Quantitative analysis of the cluster size is shown in the histo-

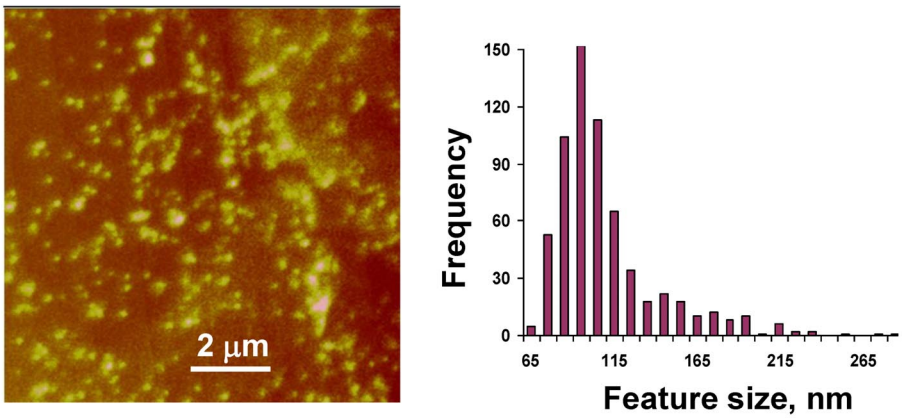

Fig. 2 NSOM (fluorescence, 488-nm excitation) image of a fixed HeLa cell, immunostained for caveolin-1. The histogram shows a quantitative analysis of the size of individual fluorescent features, giving an average diameter of 110 nm. The reported cluster sizes represent a convolution of cluster and probe diameters.

gram which gives an average diameter of 110 nm, in good agreement with the reported size of caveolae from electron microscopy [15]. These and related results demonstrate the ability of our NSOM probe design to image biological samples and indicate that NSOM has significant potential for studying membrane signaling complexes and membrane compartmentalization with resolutions that are substantially better than for diffraction-limited optical microscopy.

FCS WITH NEAR-FIELD PROBES

Initial attempts to demonstrate the feasibility of FCS measurements with near-field probes focused on measuring lipid diffusion in a supported phospholipid bilayer, as shown in the cartoon in Fig. 3 [19]. A 2D supported membrane was selected for an initial proof-of-principle experiment in order to make a direct comparison of confocal FCS with FCS-NSOM using well-known lateral-scale dimensions (i.e., by using SEM to accurately measure the probe aperture). The appropriate length scale along the optical axis is difficult to determine accurately for FCS-NSOM. This is primarily due to the uncertain contribution from the radiative component, which decays on the scale of the wavelength of light, emanating from the aperture compared to the evanescent component, which is more tightly localized, generally less than the diameter of the probe aperture for small apertures.

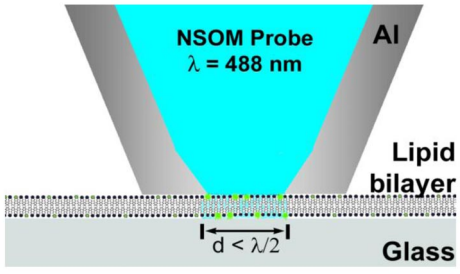

Fig. 3 Cartoon illustration of a FCS-NSOM experiment on a supported lipid bilayer, reproduced from ref. [19].

Figure 4A shows typical correlation data for diffusion of Oregon green-1,2-dihexadecanoyl-sn-glycero-3-phosphoethanolamine (OG-DHPE) in a dioleoyl-phosphatidylcholine (DOPC) bilayer on a glass cover slip measured using a near-field probe (~140-nm-diameter aperture) with excitation at 488 nm [19]. The NSOM data presented are representative of results obtained for more than 10 different probes with aperture diameters that varied between 120 and 150 nm; in most cases, FCS curves were obtained for multiple areas of several different bilayers. For comparison, Fig. 4A also shows confocal FCS data obtained for OG-DHPE in a DOPC bilayer.

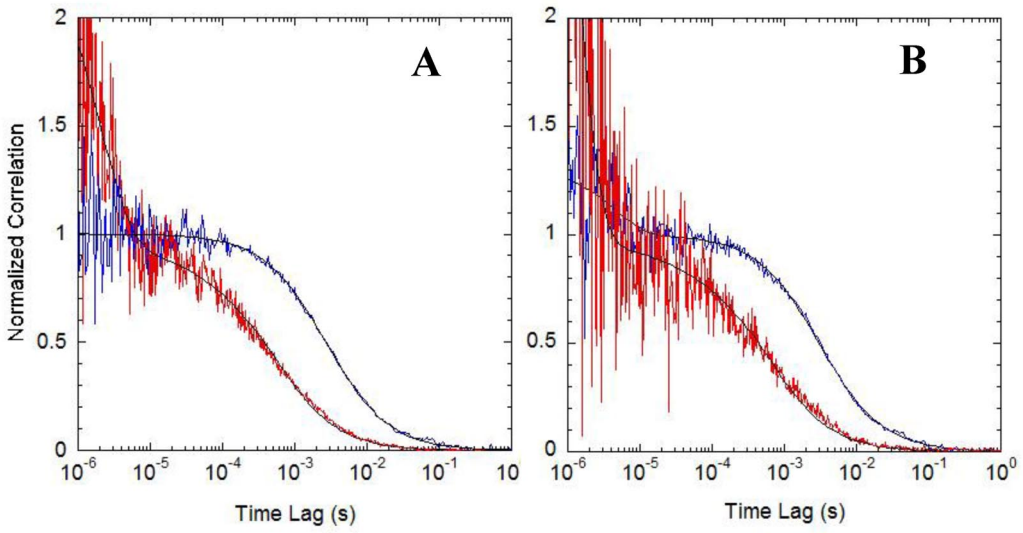

Fig. 4 Normalized correlation data for the diffusion of OG-DHPE in DOPC lipid bilayers on a glass slide (A) and mica (B) observed with near-field (blue) and confocal (red) optics. The confocal and NSOM data were fit (solid lines) assuming Gaussian and square step function observation profiles, respectively. This figure is reproduced in part from ref. [19].

Both NSOM and confocal FCS data exhibit a fast correlation decay on the 1–10 μs time-scale that is attributed to intersystem crossing, and a slow correlation decay on the millisecond time-scale due to lateral diffusion of labeled lipids within the bilayer. The NSOM curve is shifted to shorter times, as expected based on the difference in excitation area for the two methods. The confocal data are modeled assuming 2D diffusion with a Gaussian excitation profile of radius 190 nm (calibrated with fluorescein) and yield a characteristic diffusion time of $\tau = 3.3 \pm 0.3$ ms and a diffusion coefficient of $D = 2.8 \pm 0.3$ $\mu m^2/s$ [19], in excellent agreement to a published value for the same system on mica ($D = 3.1$ $\mu m^2/s$) [26].

Fitting the FCS-NSOM data requires knowledge of the excitation profile at the end of the near-field probe. Although the excitation intensity profile created by the near-field tip is not well known, it is not expected to be Gaussian [6,27], and a different model from that used for 2D diffusion using confocal optics is required to describe the correlation data acquired by FCS-NSOM. We assume that the excitation intensity is constant over the 5-nm bilayer thickness and that the probability of detecting a fluorescence photon from a fluorophore is constant directly under the aperture but falls off sharply beyond the metal-glass boundary due to the well-defined aperture, as observed in our previous work [16]. Therefore, we conclude that a circular step function is a good approximation for the radial observation profile under the near-field probe.

In order to examine the differences between Gaussian and step function profiles, correlation functions for 2D diffusion with Gaussian and circular, square, and elliptical step function observation pro-

files were calculated numerically and shown in Fig. 5 [19]. All three step function profiles are significantly stretched at fast time-scales, compared to the Gaussian profile. The early correlation decay is attributed to the sharpness of the boundary, which allows fluorophore detection for very short time periods, in agreement with previous simulations for 3D diffusion in cubic and spherical observation volumes [28]. The similarity of the correlation functions for all three step function profiles indicates that variation of the probe aperture from a perfectly circular profile will not significantly affect the FCS-NSOM results. This is an important observation since imperfections in the tip aperture frequently lead to deviations from a circular profile and polarization of the excitation beam may lead to elliptical profiles.

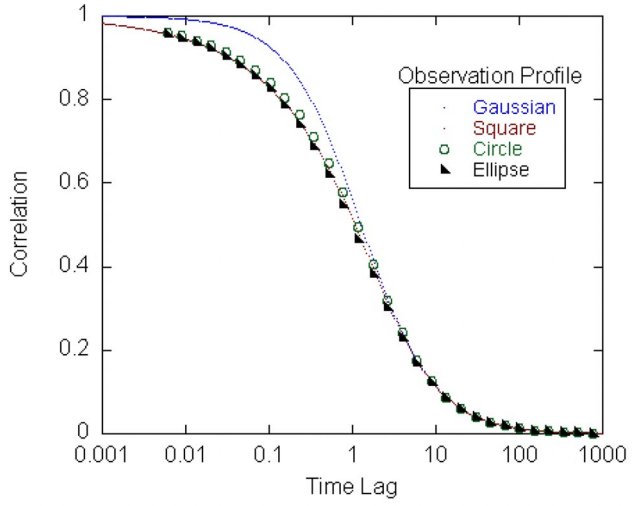

Fig. 5 Calculated 2D diffusion correlation functions (N = 1) for a Gaussian observation profile and for square, circular, and elliptical step function observation profiles, reproduced from ref. [19].

Although no analytical solution has been found for the circular and elliptical cases, the square step function observation profile can be calculated as shown in eq. 1, where $G_D(\tau)$ is the diffusional component of the correlation function, $erf(\xi)$ denotes the error function, and $\tau'_D = s^2/4D$ where s is the half-length of a side of the square for the excitation profile [19]. Equation 1 is a special case of an autocorrelation function previously derived by Thompson et al. [29]. The fit of the experimental FCS-NSOM data to eq. 1 is shown in Fig. 4 and indicates that the square step function provides a good approximation for the anticipated circular profile for the NSOM probe. This is consistent with the calculated correlation curves for which the half-time of the decay varies by only 2 % for circular and step function profiles. The FCS-NSOM data yield a characteristic diffusion time τ for the lipid of 380 ± 40 μs, an order of magnitude faster than for the confocal measurement (τ = 3.3 ± 0.3 ms). Using our measured value for the diffusion coefficient of OG-DHPE in a DOPC bilayer, we calculate the effective radius of the excitation profile to be $r = 2s/\pi^{1/2}$ = 73 nm, in excellent agreement with our measured value of the tip aperture radius (r = 70 nm). Thus, we conclude that the FCS-NSOM observation area for the probe used (0.017 μm^2) is approximately an order of magnitude smaller than in the confocal geometry (0.11 μm^2).

$$G_D(\tau) = \frac{1}{N}\left(erf\left(\sqrt{\frac{4\tau'_D}{\tau}}\right) - \frac{1}{\sqrt{\pi}}\sqrt{\frac{\tau}{4\tau'_D}}\left(1 - e^{\frac{-4\tau'_D}{\tau}}\right)\right)^2 \quad (1)$$

To show generality of the above results, FCS data were also obtained for OG-DHPE diffusion in DOPC bilayers on mica; a comparison of confocal and NSOM data is shown in Fig. 4B. The brightness per molecule even for very thin mica (~10 μm) was typically a factor of 3 lower than that for a bilayer on glass measured using the same probe, which accounts for the much poorer-quality curve for the FCS data. Nevertheless, fits of the FCS-NSOM data give the expected probe radius of 70 nm. Diffusion of NBD-DHPE in DOPC bilayers on glass was also examined and gave similar results to OG, although also with lower brightness per molecule. Experiments using phase-separated bilayers containing ordered sphingomyelin and cholesterol-rich domains surrounded by a fluid DOPC phase gave more complex correlation curves that could be fit to two diffusing species, consistent with contributions from diffusion in both ordered and fluid phase regions or the bilayer.

Comparison of the NSOM and confocal data shown in Fig. 4 suggests a similar quality of data for the two experiments. However, it is important to compare the efficiencies under matched excitation conditions. The excitation intensity at the end of a near-field probe is a combination of evanescent and propagating components, and is thus difficult to measure. Therefore, we have measured the dependence of the FCS-NSOM brightness per molecule and diffusion time on the laser intensity coupled into the NSOM probe for comparison to confocal results [19]. The usable intensity range is limited by the signal to noise at low intensity and by damage to the probe aperture at high intensity. We have observed that above a threshold intensity (which depends on aperture diameter and Al thickness), the probe aperture apparently increases in size, due to deterioration of the Al coating. Figure 6 shows SEM images of a probe tip before and after FCS-NSOM experiments performed with excitation above this threshold intensity. There is some evidence of Al melting, or at least softening, which combined with a forceful tip interaction with the surface (due to the high spring constant of the probe), effectively pounds the Al, opening the aperture. An increase in the aperture size is also confirmed by imaging fluorescent spheres before and after the FCS-NSOM experiments. Larger fluorescence count rates are obtained after probe usage.

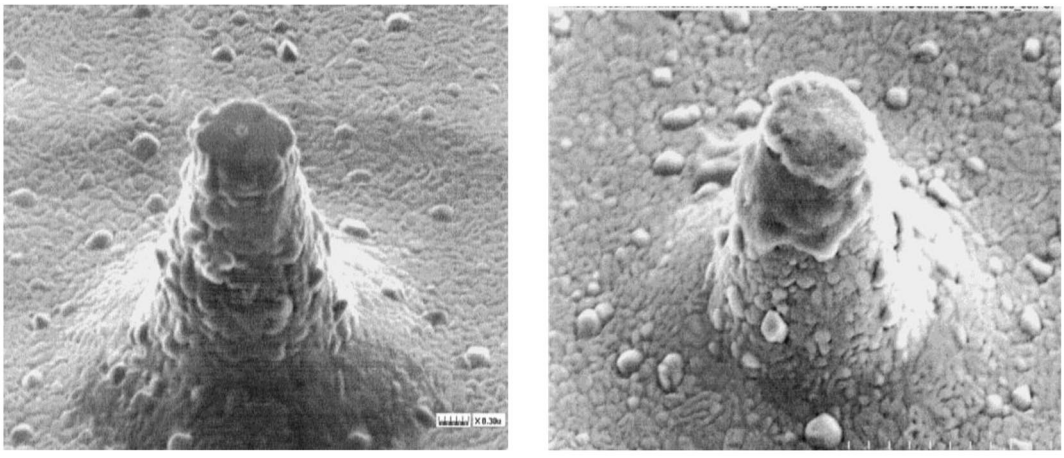

Fig. 6 SEM images of the conical structure of an NSOM probe before (left) and after (right) FCS-NSOM experiments conducted at an intensity above the threshold for damage to the probe aperture.

Variation of the laser excitation intensity over the limited range that we can examine shows no decrease in residence time with increasing intensity, indicating that photobleaching is not an issue in these experiments. This we attribute to the much shorter residence time of the molecules in the excitation volume, as compared to confocal. Furthermore, matching the triplet state photophysics observed for OG in the FCS-NSOM experiments with that observed in confocal FCS measurements indicates that the

brightness per molecule is roughly 10 times higher for confocal than for NSOM at the same excitation intensity. There are a number of possible explanations for the lower brightness per molecule in the FCS-NSOM experiments. First, use of a higher numerical aperture objective, as employed for confocal measurements, will give approximately 2.5 times improvement in light collection efficiency. Secondly, the lower brightness may partially reflect errors associated with using the triplet yield to attempt to match excitation intensities. Third, bleaching effects due to the Al coating of the probe may contribute to a lower brightness in the NSOM-FCS experiments. Clearly there is significant scope for further improvements to the efficiency of our current FCS-NSOM set-up. These include the use of a higher numerical aperture objective to improve the light collection efficiency and optimization of the NSOM probe design to allow higher excitation intensities.

SUMMARY AND PERSPECTIVES

Having demonstrated the feasibility of FCS measurements with near-field probes, it is of interest to compare this approach to other methods used to reduce the FCS excitation volume. FCS-NSOM represents a significant improvement over the untapered fiber optic-based approach, and the approximately 10-fold reduction in observation area is already larger than the reduction in volume achieved with the supercritical objective or STED methods. NSOM can achieve observation length scales similar to those obtained with fixed arrays of subwavelength holes in metal films. In the context of single-molecule dynamics for membranes, the near-field probe approach has the potential to image a membrane at high spatial resolution prior to conducting FCS measurements on targeted areas of the membrane [15–17]. This is not possible with arrays of apertures since the cells must be grown on the Al film in which the nanoapertures are fabricated and only the areas of the cell membrane that grow into the nanoapertures can be interrogated. Furthermore, we have shown that FCS-NSOM data for diffusion in a 2D supported membrane may be analyzed using a simple analytical model, in contrast to FCS in a nanoaperture which significantly perturbs the shape of the membrane and requires the use of non-analytical functions to model the data [8]. Despite the obvious advantages of near-field probes for FCS, the high spring constant and lengthy fabrication process for the current probe design will require improvements. Recent work in our laboratory has shown that reduction of the probe spring constant by a factor of approximately 10 can be achieved by reducing the diameter of the optical fiber. These probes are compatible with scanning supported membranes at higher speeds without damage (manuscript in preparation) and facilitate more routine FCS measurements.

In summary, we have demonstrated the application of near-field optical probes to achieve an FCS observation area that is an order of magnitude below the diffraction limit. It should be possible to achieve an additional order of magnitude reduction in the observation area by using probes with smaller apertures. This will enable the study of membranes with higher concentrations of fluorophores than is currently possible with diffraction-limited techniques. More importantly, FCS-NSOM has considerable potential for observations on cellular membranes, which possess submicron features such as lipid domains and macromolecular assemblies, because the small axial extent of the near-field will minimize excitation of auto-fluorescence from the cytoplasm. FCS-NSOM may also prove useful for measurements in solution and two-color FCS applications where high concentrations of solutes are often required. Two-color applications with NSOM probes will be an advantage over confocal measurements where beam overlap is frequently problematic.

REFERENCES

1. E. Haustein, P. Schwille. *Methods* **29**, 153 (2003).
2. D. Magde, E. Elson, W. W. Webb. *Phys. Rev. Lett.* **29**, 705 (1972).
3. K. Hassler, T. Anhut, R. Rigler, M. Gosch, T. Lasser. *Biophys. J.* **89**, L01 (2005).
4. J. Ries, T. Ruckstuhl, D. Verdes, P. Schwille. *Biophys. J.* **94**, 221 (2008).
5. L. Kastrup, H. Blom, C. Eggeling, S. W. Hell. *Phys. Rev. Lett.* **94**, 178104 (2005).
6. M. Leutenegger, M. Gosch, A. Perentes, P. Hoffman, O. J. E. Martin, T. Lasser. *Opt. Express* **14**, 956 (2006).
7. J. Wenger, F. Conchonaud, J. Dintinger, L. Wawrezinieck, T. W. Ebbesen, H. Rigneault, D. Marguet, P.-F. Lenne. *Biophys. J.* **92**, 913 (2007).
8. K. T. Samiee, J. M. Moran-Mirabel, Y. K. Cheung, H. G. Craighead. *Biophys. J.* **90**, 3288 (2006).
9. M. J. Levene, J. Korlach, S. W. Turner, M. Foquet, H. G. Craighead, W. W. Webb. *Science* **299**, 682 (2003).
10. J. Korlach, P. J. Marks, R. L. Cicero, J. L. Gray, D. L. Murphy, D. B. Roitman, T. T. Pham, G. A. Otto, M. Foquet, S. W. Turner. *Proc. Natl. Acad. Sci. USA* **105**, 1176 (2008).
11. J. B. Edel, M. Wu, B. Baird, H. G. Craighead. *Biophys. J.* **88**, L43 (2005).
12. H. Blom, L. Kastrup, C. Eggeling. *Curr. Pharm. Biotechnol.* **7**, 51 (2006).
13. A. Lewis, H. Taha, A. Strinkovski, A. Manevitch, R. Khatchatouriants, R. Dekheter, E. Ammann. *Nat. Biotechnol.* **21**, 1378 (2003).
14. R. C. Dunn. *Chem. Rev.* **99**, 2891 (1999).
15. A. Abulrob, Z. Lu, E. Brunette, D. Pulla, S. Stanimirovic, L. J. Johnston. *J. Microsc.* **232**, 225 (2008).
16. A. Ianoul, M. Street, D. Grant, J. Pezacki, R. Taylor, L. J. Johnston. *Biophys. J.* **87**, 3525 (2004).
17. A. Ianoul, D. D. Grant, Y. Rouleau, M. Bani-Yaghoub, L. J. Johnston, J. P. Pezacki. *Nat. Chem. Biol.* **1**, 196 (2005).
18. K. Garai, R. Sureka, S. Maiti. *Biophys. J.* **92**, L55 (2007).
19. D. Vobornik, D. S. Banks, Z. Lu, C. Fradin, R. Taylor, L. J. Johnston. *Appl. Phys. Lett.* **93**, 163904 (2008).
20. P. Burgos, Z. Lu, A. Ianoul, C. Hnatovsky, M.-L. Viriot, L. J. Johnston, R. S. Taylor. *J. Microsc*. **211**, 37 (2003).
21. R. S. Taylor, J. Li, M. Phaneuf. "Comparison of focussed ion-beam hole drilling and slicing for NSOM aperture formation", in *Near-field Optics: Principles and Applications, 2nd Asia-Pacific Workshop on Near Field Optics*, X. Zhu, M. Ohtsu (Eds.), pp. 181–187, World Scientific, Beijing (1999).
22. E. X. Jin, X. Xu. *J. Microsc.* **229**, 503 (2007).
23. P. Burgos, C. Yuan, M.-L. Viriot, L. J. Johnston. *Langmuir* **19**, 8002 (2003).
24. A. Ianoul, P. Burgos, Z. Lu, R. S. Taylor, L. J. Johnston. *Langmuir* **19**, 9246 (2003).
25. J. Murray, L. Cuccia, A. Ianoul, J. C. Cheetham, L. J. Johnston. *ChemBioChem* **5**, 1 (2004).
26. M. Przybylo, J. Sykora, J. Humpolickova, A. Benda, A. Zan, M. Hof. *Langmuir* **22**, 9096 (2006).
27. J. A. Veerman, M. F. Garcia-Parajo, L. Kuipers, N. F. Van Hulst. *J. Microsc.* 477 (1999).
28. J. A. Dix, E. F. Y. Hom, A. S. Verkman. *J. Phys. Chem. B* **110**, 1896 (2006).
29. N. L. Thompson, T. P. Burghardt, D. Axelrod. *Biophys. J.* **33**, 435 (1981).